ELSEVIER

Applied Surface Science 102 (1996) 350–359

applied surface science

Theory of silicon nanostructures

Alex Zunger *, Lin-Wang Wang

National Renewable Energy Laboratory, Golden, CO 80401, USA

Abstract

Empirical pseudopotential plane wave theory is used to study the electronic and optical properties of thousand atom hydrogen passivated Si quantum dots, wires and films. The properties studied include: (1) band gap vs. size; (2) band gap vs. shape; (3) total electronic density of state and optical absorption spectra; (4) dielectric constant vs. size. The results are compared with tight binding and other model calculations. Comparison with recent experimental data is discussed.

1. Introduction

Effective mass based methods have been used traditionally to describe nanostructures. We will treat instead nanostructures with the same level of sophistication possible for bulk solids, namely an all-band pseudopotential technique. We will thus describe the electronic structure of nanostructures in terms of solutions to an effective single-particle Schrödinger's equation:

$$\hat{H}\psi_i = \epsilon_i \psi_i \tag{1}$$

where $\hat{H} = -\frac{1}{2}\nabla^2 + V(\mathbf{r})$ and $V(\mathbf{r})$ is the mean-field potential. This potential is represented as a superposition of atom-centered quantities:

$$V(\mathbf{r}) = \sum_{\text{atom}} v_{\text{atom}}(\mathbf{r} - \mathbf{R}_{\text{atom}}) \tag{2}$$

and the wavefunctions are expanded in plane waves

$$\psi_i(\mathbf{r}) = \sum_{\mathbf{q}} a_i(\mathbf{q})\, e^{i\mathbf{q}\cdot\mathbf{r}} \tag{3}$$

Here, $\{\mathbf{R}_{\text{atom}}\}$ are atomic position vectors and $a_i(\mathbf{q})$ are variationally determined expansion coefficients at the reciprocal lattice vector $\mathbf{q}$ of the supercell. Notice that we do not use the effective mass, or the envelope function approximation.

Modelling of such 10^3 atom systems using Eqs. (1)–(3) requires three steps:

First, one needs to model the geometry, i.e., to specify $\{\mathbf{R}_{\text{atom}}\}$. Experimental structural measurements on > 100 atom Si quantum dots [1] show that the atomic positions and the interatomic distances in the interior of the quantum dots are very close to the values of the extended bulk solid. Atomic relaxations exist only near the surface. We will model such relaxations using first-principle calculations and experimental data on the relevant *bulk surfaces*.

Second, one needs to calculate the potentials $v_{\text{atom}}(r)$. We use for this purpose the empirical pseudopotential method [2] (EPM). Rather than fit $v_{\text{atom}}(\mathbf{G}_i)$ at a few discrete reciprocal lattice vector $\{\mathbf{G}_i\}$ of the primary unit cell (as done in classic bulk EPM calculations [2]), we fitted a continuous $v_{\text{atom}}(q)$ to a series of experimental data and to detailed first-principles calculations on relevant prototype systems. Unlike the case in tight-binding approaches, we are able to compare the ensuing potential $V(\mathbf{r})$ with screened first-principles local density approxi-

* Corresponding author. Fax: +1 303 3846531; e-mail: alexzunger@nrel.gon.

PII S0169-4332(96)00078-5

mation (LDA) results. Unlike the case with the LDA, we are able to obtain experimentally sensible excitation energies. The pseudopotential fitting procedure is described in detail in Ref. [3].

The third step involves solving Eq. (1) for a given geometry and potential. This is nontrivial for 1000 atom systems. For most semiconducting systems made up of main group elements, one needs about 50 plane waves per atom. So for $N = 1000$ atoms, one typically has a $50\,000 \times 50\,000$ Hamiltonian problem. The conjugate gradient approaches to this problem scales as N^3, so large systems can not be treated, if all occupied eigenstates of Eq. (1) are to be calculated. However, we may not need all eigenstates in order to study, e.g, the threshold optical properties of semiconductor quantum structures. What one typically needs to know on such systems includes: (a) the eigenvalues and eigenfunctions of the band edge states (the valence band maximum, VBM and the conduction band minimum, CBM); (b) the total and local electronic density of states; (c) the optical absorption spectra. With these three properties calculated, most of the optical characteristics of the system can be determined. We have designed two new methods [4,5] to calculate these properties. First, the 'folded spectrum method' [4] calculates the band edge states with an effort that scales as $O(N)$. Second, the 'generalized moments method' [5] calculates the density of states and optical absorption spectra. Full details of these computational methods are given in Ref. [4] and [5].

2. Application to Si nanostructures

2.1. Dependence of the band gap on size for Si spheres, cubes and rectangular boxes

The most commonly addressed question in quantum dot physics is the size dependence of the energy gap. However, experimentally prepared quantum dots not only have different sizes, but for each size there could be a distribution of shapes. We study here three 'prototype shapes': (i) spherical balls, (ii) rectangular boxs [the surfaces are in the (110), (1$\bar{1}$0) and (001) directions and the lengths of the edges satisfy $d_x = d_y = d_z/\sqrt{2}$] and (iii) cubic boxes [the surfaces are in the (001), (010), (100) directions]. To compare the electronic properties of these different prototype shapes, we need a consistent definition of the quantum dot's size. A natural choice is to associate the effective size with the diameter of a sphere which has the mass density ρ of bulk Si and contains the same number N of silicon atoms as the quantum dot in question. Then the diameter is

$$d(N_{Si}) = (3/(4\pi\rho))^{1/3} N_{Si}^{1/3} = 3.3685 N_{Si}^{1/3} \text{ (Å)}$$

and the radius $R = d/2$. Using this definition, the calculated size dependence of the CBM–VBM band gaps of the three prototype quantum dots is depicted as symbols and the solid line in Fig. 1. Quite surprisingly, the three sets of data corresponding to the three prototype quantum dot shapes collapse into a single, unified curve. Thus, if we measure the effective size by $d \propto N_{Si}^{1/3}$ and vary N_{Si}, the gaps of all prototype shapes (which are not too prolate) fall on a 'universal' curve. Expressing d in Å, this curve can be fitted as:

$$E_g(d) = 1.167 + 88.34/d^{1.37} \text{ (eV)} \quad (4)$$

2.2. Quantum dot wavefunctions and the role of surface atoms

It is commonly thought that since the surface-to-volume ratio increases rapidly as the quantum dot

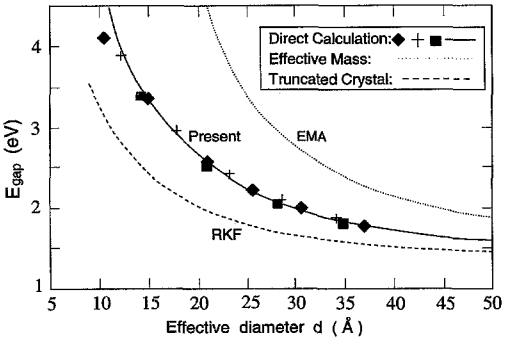

Fig. 1. CBM-VBM band gap (without Coulomb corrections) versus the effective diameter $d = 3.3685 N_{Si}^{1/3}$ (Å) for three prototype quantum dot shapes. The symbols ◇, +, and □ stand for the spheres, (110)×(1$\bar{1}$0)×(001) rectangular boxes, and (100)×(010)×(001) cubic boxes, respectively. The fitted solid line is given by Eq. (4). Also shown are the multiband effective mass result (EMA) (Ref. [6]) and the result of the method of Rama Krishna and Friesner (RKF) (Ref. [7]) [applied here to cubic quantum dots with the present Si pseudopotential]. In all cases, the excitonic Coulomb energy is excluded.

decreases, this must imply a greater role of surface effects on the electronic structure. This is true only if the wavefunction has an amplitude on the surface atoms. We test this next.

Shown in Fig. 2a,b are the wavefunction square of the CBM and VBM of the rectangular quantum box with $d = 34.1$ Å ($N_{Si} = 1035$ atoms). The VBM and CBM states are found to be localized in the interior of the quantum dot, with zero amplitude on the surface. Because of this and the fact that hydrogen potential is of very short range, we find that, as long as all dangling bonds are passivated, the details of the surface passivating atoms play little direct role in the determination of the wavefunctions, hence the band gaps and the oscillator strengths.

2.3. Comparison of the band gaps with previous calculations

Fig. 1 compares the results of two model calculations with our *direct* ('exact') calculations. These models includes the multiband effective mass approximation (EMA) of Takagahara and Takeda [6] and the model of Rama Krishna and Friesner (RKF) [7].

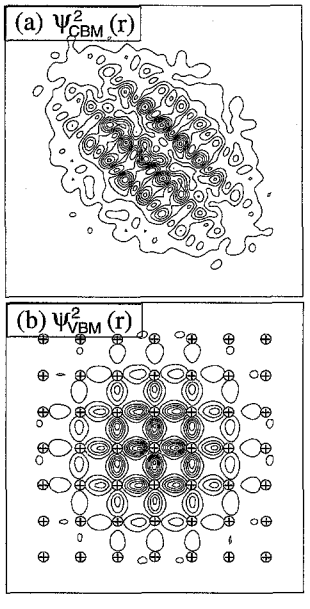

Fig. 2. Wavefunction square contour plots of the $(110)\times(1\bar{1}0)\times(001)$ rectangular quantum box with $d = 34.1$ Å and $N_{Si} = 1035$ viewed from the [001] direction. (a) The CBM wavefunction square summed along the z direction. (b) The VBM wavefunction square plotted on the $z = d_z/2$ cross section. The crossed circles in (b) denote the positions of the silicon atoms on that plane.

2.3.1. Comparison with the effective mass method

As could be seen in Fig. 2, the VBM and CBM states found in our direct calculations are not surface states, hence a comparison with the results of the (surfaceless) EMA is warranted. Our 'exact' calculation result of Eq. (4) gives a $1/d^{1.37}$ size scaling, while the effective mass model predicts a $1/d^2$ scaling. Hence, the parabolic dispersion assumed in the EMA is inadequate in the range of quantum dot sizes studied here ($d < 40$ Å), despite the fact that multiband coupling is correctly included in this EMA calculation. Indeed, the effective mass approximation (which includes only kinetic energy effects neglecting explicit potential energy within the dot) exaggerates considerably the increase of band gap $[\Delta E_g(d) = E_g(d) - E_g^{bulk}]$ with reduced size. Replacing in the EMA calculation the infinite wall by a finite barrier reduces $\Delta E_g(d)$ and softens the $1/d^2$ scaling. Solving the EMA equation for a finite barrier of height 4 eV and using an effective mass $m^* = 0.2m$ gives a 10% lower $\Delta E_g(d)$ for $d = 40$ Å and a 15% lower $\Delta E_g(d)$ for $d = 25$ Å. This reduces the EMA error relative to our direct calculations by 20% and 30% for $d = 40$ and 25 Å, respectively. The remaining, bigger part of the error must come from (i) the EMA Hamiltonian itself, i.e, from the assumption of parabolic dispersion, and (ii) possible nonabruptness of the potential well.

Zunger et. al. [8] have extended the comparison of (single band) effective mass vs. pseudopotential method to Si wires and films. The results are shown in Fig. 3. We see that the EMA overestimates significantly the quantum confinement shift $\Delta E_i(d) = E_i(d) - E_i(\text{bulk})$ and that the order of the EMA errors is $\delta\Delta E(\text{box}) > \delta\Delta E(\text{wire}) > \delta\Delta E(\text{film})$ (Fig. 3b). Note that the error is smallest for 2D films (in vacuum), and is probably still smaller in 2D quantum wells (embedded in a barrier). This explains partly the success of the EMA in quantum wells, but warns against the hope that similar success will be carried over to wire and dots. Note also from Fig. 3a that the size dependence of the quantum confinement is the weakest fot film (d^{-n} with $n \approx 0.8$ compared to $n \approx 1.3$ for wires). Thus, if one wants to make a 2

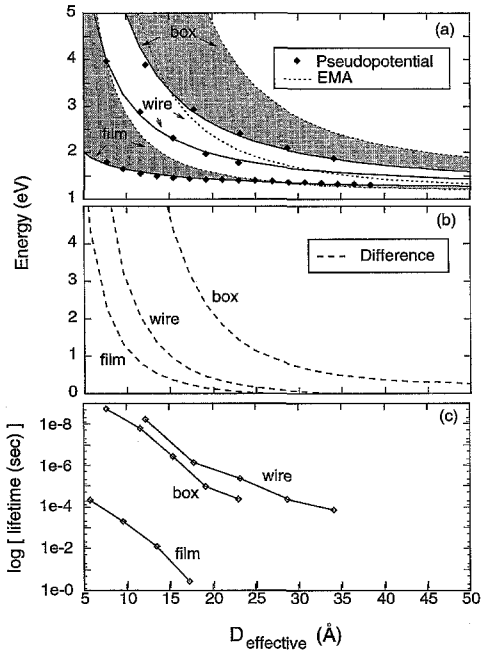

Fig. 3. Energy gaps (a), absolute EMA errors in the band gap (b) and radiative lifetimes (c) for H-covered Si films, wires and boxes. The surface orientations are (110) for films, (110)×($\bar{1}$10) for wires, and (110)×($\bar{1}$10)×(001) for boxes. We use $D_{\text{eff}} = D_{110}$ for films, $D_{\text{eff}} = D_{110} = D_{110}$ for wires and $D_{\text{eff}} = 3.369 N_{\text{Si}}^{1/3}$ for boxes, where N_{Si} is the number of Si atoms and D_{110} is the H surface layer to H surface layer distance in (11) direction. This figure is taken from Ref. [8].

eV gap Si system, one needs a ~ 5 Å film or a ~ 20 Å wire or a ~ 32 Å dot.

It is interesting to note that in 2D quantum films, the effective mass method leads not only to quantitative but also to qualitative errors. This is illustrated in Fig. 4. While in the EMA the energy levels vary monotonically with size, the EPM solutions for (001)-oriented quantum films (Fig. 4a) show non-monotonic (even–odd) oscillations in the valence band energies. The amplitude of these oscillations is reduced somewhat when the film's surface is covered by hydrogen (Fig. 4b). No oscillations exist in (110) oriented films. The EMA fails quantitatively in describing the valence band states (in either cases: clean or H covered surfaces) for film's thickness below ~ 20 Å. The reason is that the EMA fails to recognize the changes in symmetry in going from an even to an odd number of atomic layers: EMA has only the film thickness as its parameter. The EPM solutions of a hydrogen-free (001) quantum film exhibit a VBM state whose energy does not change with film thickness (see even-layers in Fig. 4a). This 'zero confinement state' (ZCS) is missing in the EMA result. The ZCS corresponds to a cosine-type envelope function which is forbidden in EMA. But it is allowed in the EPM calculation because the boundary condition is satisfied by the Bloch function, not by the envelope function. The ZCS energy becomes unpinned under H chemisorption (Fig. 4b) and in (110) films. It is absent in wires and boxes.

2.3.2. *Comparison with the method of RKF*

In the method of Rama-Krishna and Friesner (RKF), the cluster eigenvalues E_i^{dot} are approximated by bulk band structure energies, $E_n^{\text{bulk}}(k^*)$ at the k^*-point of a particle-in-a-box model, i.e $E_i^{\text{dot}} \cong E_n^{\text{bulk}}(k^*)$. In general, however, more than one band is needed to describe a quantum dot wavefunction. Fig. 1 shows that the method of RKF [7] underestimates the band gap opening $\Delta E(d)$. The reason for this is the neglect of band mixing.

It is significant that the single-band approximation

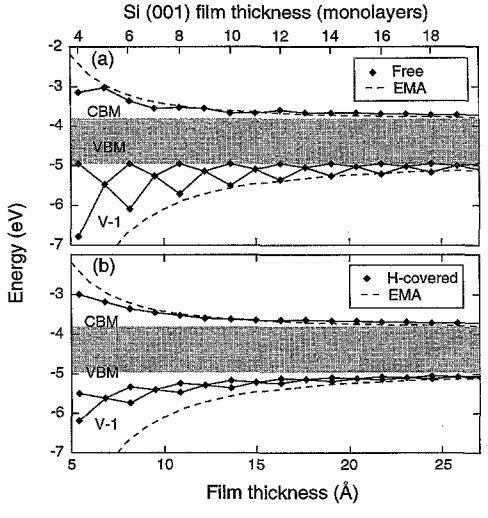

Fig. 4. Calculated near-gap energy levels of (001) oriented hydrogen free (a) and hydrogen covered (b) Si films. All states shown are bulk-like (i.e., surface states in (a) are omitted). Note the oscillations in the highest occupied (VBM) and the next-highest occupied (V − 1) valence bands, absent in the EMA description (dashed line). The zero-confinement state having a size independent energy is apparent in (a). This figure is taken from Ref. [8].

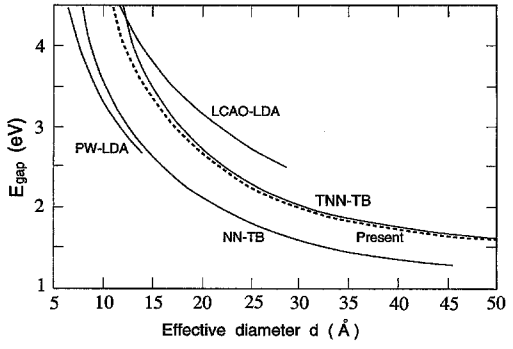

Fig. 5. Comparison of calculated CBM-VBM band gaps vs. size as obtained with different direct calculation methods. The curve representing the current results is the fitted curve of Eq. (4). The other results are NN-TB (nearest neighbor tight-binding) from Ref. [10], TNN-TB (third nearest neighbor nonorthogonal basis tight-binding) from Ref. [11], LCAO-LDA from Ref. [12] and PW-LDA (plane wave LDA) from Ref. [13]. See text for detail discussions.

of RKF underestimates the band gap. In a recent paper [9], the authors noted that the experimental observation of an unusually low band gap for Si dots (see Fig. 10 below) supports their model. However, improving their model by allowing coupling with other bands shifts their band gap upwards significantly (by ~ 0.6 eV for $d = 20$ Å see Fig. 1), thus removing the claimed agreement with experiment. Further analysis of experiment is thus needed.

2.3.3. Comparison with other direct calculations

Fig. 5 compares our results for E_g vs. d with four previous direct calculations: the empirically fitted nearest neighbor tight-binding (NN-TB) model of Ren and Dow [10], the empirically fitted third neighbor (nonorthogonal) tight-binding (TNN-TB) model of Proot, Delerue and Allan [11], and two LDA calculations: one which uses a small LCAO basis (LCAO-LDA) by Delley and Steigmeier [12] and one which uses a plane wave basis (PW-LDA) by Hirao, Udo and Murayama [13] (limited to small $N_{Si} \leq 123$ quantum dots). In all calculations, an ideal atomic structures was assumed.

The comparison of Fig. 5 shows the following: (i) the PW-LDA calculation underestimates the band gap since the intrinsic LDA band gap error was not corrected. (ii) The small basis LCAO-LDA results appear to be inaccurate. Delley and Steigmeier have subsequently improved their basis set by adding d polarization functions basis [14] and applied a 0.6 eV rigid upward shift to the calculated results to compensate the LDA band gap error. Their new results agree perfectly with our results. (iii) The two TB models differ essentially by a constant shift. Our results agree closely with the TNN-TB, indicating that longer than nearest neighbor interactions and basis set overlap effects are important.

It is significant that tight-binding methods using but a few neighbor matrix elements (e.g NN-TB in Fig. 5) underestimate the calculated band gap relative to better converged TB calculations (e.g, TNN-TB). In this respect we note that the better agreement of the TB calculations of Hill and Whaley [15] with the very low experimental band gap could represent a fortuitous effect of an underconverged TB representation.

2.4. Density of states and optical absorption spectra

The total and surface local density of states of the spherical quantum dots calculated by the generalized moment method are shown in Fig. 6, while Fig. 7 shows the corresponding optical absorption spectrum. The DOS and optical absorption spectrum of the largest spherical dot $Si_{1315}H_{460}$ already resemble some of the features of their bulk counter parts. On

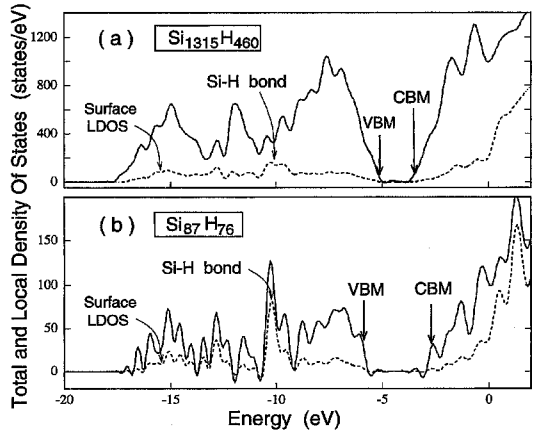

Fig. 6. Calculated total and local density of states of spherical Si quantum dots. The vertical arrows denote band edge state positions calculated by the folded spectrum method. The zero of the energy is the vacuum level. (a) $Si_{1315}H_{460}$, (b) $Si_{429}H_{228}$, (c) $Si_{87}H_{76}$.

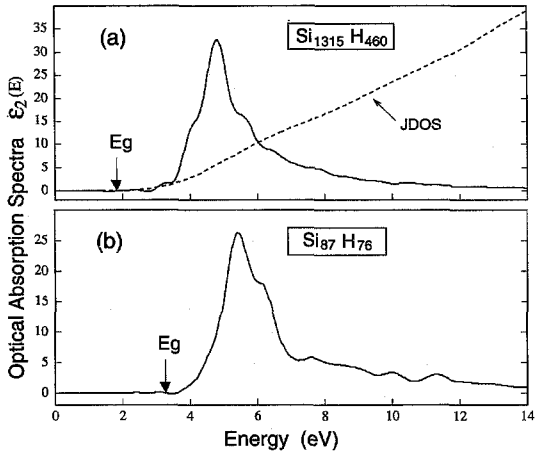

Fig. 7. Calculated optical absorption spectra $\epsilon_2(E)$ of spherical Si quantum dots. (a) $Si_{1315}H_{460}$, (b) $Si_{429}H_{228}$, (b) $Si_{87}H_{76}$. The joint density of states (JDOS) in (a) is given in arbitrary units. The vertical arrows denote the band gap values calculated by the folded spectrum method.

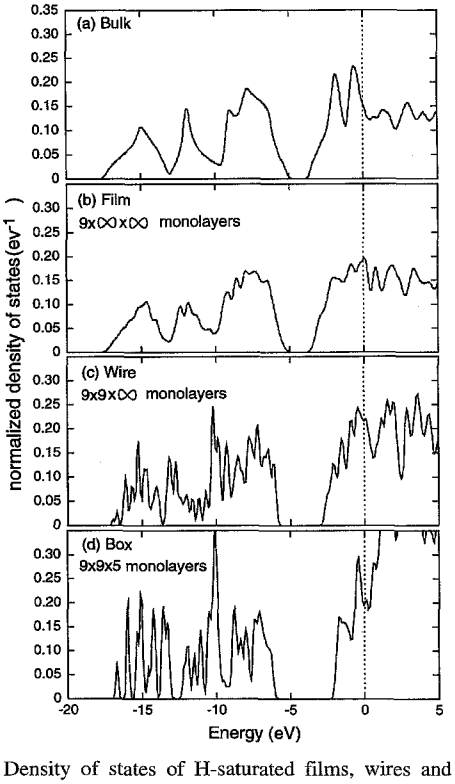

Fig. 8. Density of states of H-saturated films, wires and boxes with surface orientations denoted in the caption of Fig. 3. They are normalized so that the integral of the valence electrons equals 1. Gaussian broadening is 0.2 eV. This figure is taken from Ref. [8].

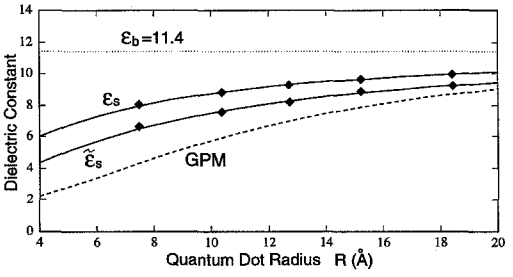

Fig. 9. Dielectric constants as a function of spherical quantum dot radius R. Here ϵ_s is for total polarization and $\tilde{\epsilon}_s$ is for exciton screening. The diamond symbols are the calculated results while the solid lines are the curves fitted to Eq. (5). The dashed curve corresponds to the generalized Penn model (GPM) given by Ref. [17].

the other hand, the smaller systems show molecular features (more peaks). The calculated surface local DOS in Fig. 6 show peaks caused by Si–H bonding.

An analogous calculation of the density of states has been performed for quantum wires and films (Fig. 8). The density of states of films (Fig. 8b) is rather similar to that of the bulk (Fig. 8a) while wires (Fig. 8c) show sharp features which evolve into molecular-like states in q quantum dot (Fig. 8d). The electron affinity (distance frin vacuum level 0 to the CBM) decreases in the series film → wire → dot.

2.5. Dielectric constant and exciton screening

The integral $\epsilon_s = \int \epsilon_2(E)/E^2 \, dE$ of the optical absorption spectra $\epsilon_2(E)$ shown in Fig. 7 gives the static dielectric constant ϵ_s. Fig. 9 shows ϵ_s vs. the quantum dot diameters. This dielectric constant measures the total polarization response $\mathbf{P}$ of a quantum dot to a constant total electric field $\mathbf{F}$:

$$\epsilon_s \equiv 1 + \mathbf{P}/\mathbf{F}\Omega,$$

where Ω is the volume of a quantum dot. We also show the dielectric constant $\tilde{\epsilon}_s$ which governs the screening of the exciton in a quantum dot (Ref. [16]). $\tilde{\epsilon}_s(R)$ is smaller than $\epsilon_s(R)$ as expected from the q dependence of the bulk $\epsilon(q)$ [1]. Also plotted in Fig. 9 is the dielectric constant predicted from a generalized Penn model [17] (GPM). This model predicts a

[1] The $\epsilon_s(R)$ is analogue to $\epsilon_{bulk}(q=0)$ and $\tilde{\epsilon}_s(R)$ is analogue to $\epsilon_{bulk}(q \approx \rho/R)$ in the bulk.

value much smaller than $\epsilon_s(R)$ and $\tilde{\epsilon}_s(R)$. The result of the GPM can be expressed as

$$\epsilon_s(R) = 1 + \frac{\epsilon_b - 1}{1 + (\alpha/R)^l} \quad (5)$$

with $l = 2$ and $\alpha = 10.93$ Å, where $\epsilon_b = 11.4$ is the Si bulk dielectric constant. Fitting our directly calculated results to the same form, we find $l = 1.25$, $\alpha = 4.25$ Å for our total polarization dielectric constant ϵ_s and $l = 1.37$, $\alpha = 6.9$ Å for our screening dielectric constant $\tilde{\epsilon}_s$. [Note, however, that Eq. (5) with $l < 2$ can be used only for finite clusters since $l = 2$ is the rigorously correct scaling for $R \to \infty$.] Using the generalized Penn model, the ratio between the free exciton radius a_{eh} and the quantum dot dimension is very close to one, thus the system is predicted to experience 'moderate confinement'. On the other hand, the ratio obtained in our microscopic calculation is much larger than one, indicating strong confinements. Recently Lannoo and Allen [18] calculated ϵ vs. size using a tight-binding based self-consistent linear screening method, finding even slightly larger suppression of the dielectric constant with size than found here.

2.6. Comparison of calculated exciton energy with experiment

Having calculated the intrinsic one-electron CBM-VBM band gap $E_{gap}(R)$ (Fig. 1) and the screening dielectric constant $\tilde{\epsilon}_s(R)$ for the Coulomb energy (Fig. 9), we are now in a position to compare our exciton energy to experimental data.

In order to compare with the experimental data, the Coulomb interaction energy between the excited electron and the hole is added to the calculated intrinsic band gap E_{gap}. This gives the exciton energy for a sphere within infinite barrier as [19] (in atomic unit, Hartree for energy, Bohr radius for R):

$$E_x(R) = E_{gap}(R) - \frac{1.786}{\tilde{\epsilon}_s(R)R} - 0.248\,E_{Ry} \quad (6)$$

The second term in Eq. (6) is the Coulomb energy, while the third term is a correlation energy correction with $E_{Ry} = 8.18$ meV.

We first compare our result with the band gaps estimated using the optical absorption spectrum [20,21]. The comparison is shown in Fig. 10a. Our results, and those using the TNN-TB (Ref. [11]) agree well with experiment for their trends, except that the excitonic correction [second term of Eq. (6)] seems too large, by ca. 0.2 eV, so the calculated $E_x(R)$ is slightly below experiment.

We next compare our result with photoluminescence (PL) spectra [1,22–24] in Fig. 10b. The size distribution is measured by high-pressure-liquid chromatography, transmission electron microscopic and X-ray peak width. Our calculated result is systematically above the experimental PL data.

Unfortunately, the comparisons in Fig. 10 are somewhat obscured by experimental uncertainties: In both absorption and PL experiments, there is large size distribution. In the absorption experiments, due to the indirect gap nature of the material, there are

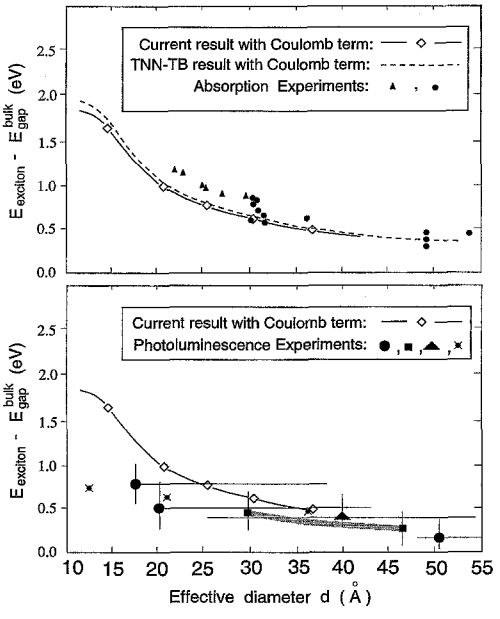

Fig. 10. Calculated excitonic energy [Eq. (6)] compared with (a) experimental band gap from absorption measurement (b) PL energy for spherical quantum dots. The symbols ○, △ in (a) denote data from Ref. [20,21], respectively. The dashed line in (a) denote the TNN-TB calculated results from Ref. [11]. However, unlike in Ref. [20], here the Coulomb energy using $\tilde{\epsilon}_s(R)$ has been added to the TNN-TB calculated $E_{gap}(R)$ in Eq. (6). The symbols ○, △, □ and x in (b) denote PL data from Ref. [1,22–24], respectively. The vertical lines in (b) represent the widths at half-maximum of the PL spectra. The horizontal lines in (b) denote the estimated size distributions.

further complications in determining the exact band gap from the absorption spectra. Thus we decided as a 'sanity test' to compute the excitonic gap vs. size [25] for a system for which the experimental data are much more accurate CdSe dots. In the case of CdSe [26], the size can be controlled within 5% and the exciton energy is measured from an exciton peak in the absorption spectrum (due to the direct band gap nature of CdSe). We use the same methodology, the same type of carefully fitted empirical pseudopotential [3]. We found [25] that our methodology produces excellent agreement with experiment for CdSe.

Thus, we conclude that our methodology should produce reliable results. Based on this, and the facts that our calculated exciton energy is systematically higher than the experimental photoluminescence energy at small quantum dot sizes, we conjecture that in Si dots the photoluminescence originates from some persistent (approximately size-independent) defects or impurities states (e.g, surface states), rather than from intrinsic dot states. This is also supported by the fact that the experimental absorption spectrum gap in Fig. 10a is systematically larger than the experimental photoluminescence energy in Fig. 10b.

A different type of experiment [27] is, however, uncomplicated by the uncertainty in size distribution and possible surface defect states. In this experiment, the size-induced shift ΔE_v in the top of valence band and the shift ΔE_c in the bottom of conduction band are measured from absorption spectra for porous silicon of different quantum dot sizes:

$$\Delta E_v(d) = E_{VBM}(\text{bulk}) - E_{VBM}(d)$$
$$\Delta E_c(d) = -E_{CBM}(\text{bulk}) - E_{CBM}(d) \quad (7)$$

Instead of focusing on the highly uncertain size dependence, the ratio ΔE_v vs. ΔE_c plots are given, thus obviating the need of measuring the size. $\Delta E_c(R)$ and $\Delta E_v(R)$ are plotted in Fig. 11. As shown in Fig. 11, if the bulk dielectric constant $\epsilon_b = 11.4$ is used instead of $\tilde{\epsilon}_s(R)$, the result deviates considerably from the experimental data. The reasonable agreement with experiment suggests that when the measured dot size is not used, theory explains experiment rather well.

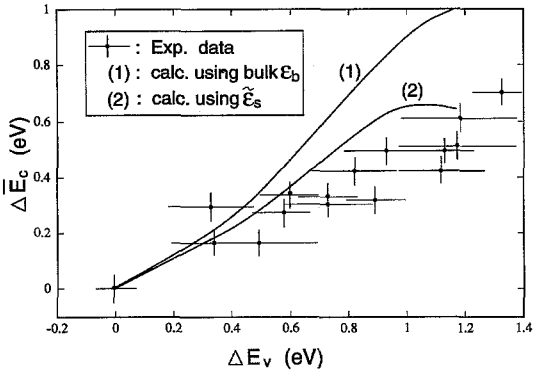

Fig. 11. Conduction band edge shifts versus valence band edge shifts. The experimental data is from Ref. [27]. The experimental conduction band shift $\Delta\tilde{E}_c = \Delta E_c(d) - 3.572/d\tilde{\epsilon}_s(d)$, where $\Delta E_c(d)$ and the Coulomb energy $-3.572/\tilde{\epsilon}_s(d)$ are given by Eq. (6).

2.7. Shape dependence at constant size

Quantum confinement effects can exist in one dimension (film), two dimension (wire) and three dimension (particle) systems. In Fig. 1, we showed that if the effective size is measured as $d \propto N_{Si}^{1/3}$, the band gap vs. size (or N_{Si}) curves are similar for three prototype shapes, for which the structures are not too prolate. It would be interesting to study the band gap change when a quantum dot goes through an extreme shape change, e.g, from a film-like object to a wire-like object. We examined this by changing the aspect ratio $d_z/d_x = d_z/d_y$ of a rectangular box (see inserts to Fig. 12): When the ratio $d_z/d_x \ll 1$, the quantum dot is film-like, when $d_z/d_x = 1$, the quantum dot is cubic, while when $d_z/d_x \gg 1$, the quantum dot is wire-like. To eliminate the effects of orientation, we studied boxes with fixed surface orientations [(100),(010),(001)] for all d_z/d_x ratios. To eliminate the effect of size N_{Si}, we studied quantum dots having almost the same number $N_{Si} = 1108 \pm 13$ of Si atoms. Fig. 12 depicts the calculated recombination rate (part a) and band gap energy (part b) versus the ratio d_z/d_x. Note that different shapes at $N_{Si} \cong$ const can have gaps that differ by as much as 0.8 eV! The structure with the smallest band gap (i.e, weakest quantum confinement effect) occurs when $d_z/d_x = 1$ (cubic). From $d_z/d_x = 4$ to 14, there is a switch between the near VBM states, as a result, the trend of the recombination rate has been changed. While the most elongated 1100-atom

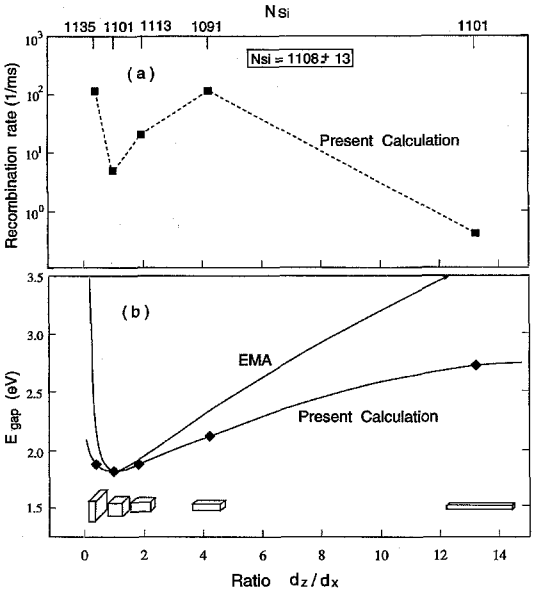

Fig. 12. Dependence of the band gap and recombination rate $(1/\tau)$ on the shape $(d_z/d_z = d_z/d_y)$ of Si quantum boxes. The box has the (100)×(010)×(001) orientation. The ratio d_z/d_x changes from 0.38 to 13.2 and the box changes from filmlike to wirelike. (a) The radiative recombination rate $(1/\tau)$ vs. ratio d_z/d_x. (b) The band gap as the ratio d_z/d_x. Fitting the $d_z/d_x = 1$ point to an EMA formula shows that when d_z/d_x differs from 1, the effective mass formula overestimates the quantum confinement effects. This is consistent with the results of Fig. 9 which indicates that the smaller the length d_x or d_z, the larger the error of the EMA.

bar gives the largest blue shift, interestingly the cube has a faster decay (i.e, the transition is 'more allowed') than this most elongated bar. Thus, a larger blue shift comes, unfortunately, with a weaker transition.

3. Conclusions

We have introduced a new approach for electronic structure calculations of nanoscale quantum systems. A plane wave basis is used to describe the wavefunctions and accurate empirical pseudopotentials are used to approximate the Hamiltonian. The empirical pseudopotentials (of continuous forms in reciprocal space) are fitted to the bulk band structure and surface density of states. The shapes of first principle LDA screened potentials are also taken into account in the empirical pseudopotential fitting. As a result, our fitted potential $V(\mathbf{r})$ is very close to LDA screened potential, except that our potential gives the correct bulk band gap and band structure, while the LDA potential does not. Our central approximation is the use of a fixed, nonself consistent potential for all dots. Two newly developed methods, the folded spectrum method and the generalized moments method, are used to calculate the band edge states, density of states and optical absorption spectra of thousand atom systems. These three quantities are sufficient to determine most optical characteristics of the system. The current approach is illustrated for Si quantum dots with surface passivation of H atoms. Recently, this approach has also been used in the study of ca. 300 nm disorder superlattices [28] and CdSe quantum dots [25].

Acknowledgements

We would like to thank S.B. Zhang and C.Y. Yeh for many helpful discussions. This work was supported by the office of Energy Research, Materials Science Division, US Department of Energy, under Grant DE-AC02-83CH10093.

References

[1] K.A. Littau, P.J. Szajowski, A.J. Muller, A.R. Kortan and L.E. Brus, J. Phys. Chem. 97 (1993) 1224.
[2] M.L. Cohen and J.R. Chelikowsky, Electronic Structure and Optical Properties of Semiconductors (Springer, Berlin, 1988).
[3] L.W. Wang and A. Zunger, Phys. Rev. B 51 (1995) 17398.
[4] L.W. Wang and A. Zunger, J. Chem. Phys. 100 (1994) 2394.
[5] L.W. Wang, Phys. Rev. B 49 (1994) 10154.
[6] T. Takagahara and K. Takeda, Phys. Rev. B 46 (1992) 15578.
[7] M.V. Rama Krishna and R.A. Friesner, Phys. Rev. Lett. 67 (1991) 629; J. Chem. Phys. 96 (1992) 873.
[8] A. Zunger, C.Y. Yeh, L.W. Wang and S.B. Zhang, in: Proc. 22nd Int. Conf. on the Physics of Semiconductors, Vancouver, Canada, Ed. D.J. Lockwood (World Scientific, Singapore, 1995) p. 1763.
[9] A. Tomasulo and M.V. Rama Krishna, unpublished.
[10] S.Y. Ren and J.D. Dow, Phys. Rev. B 45 (1992) 6492.
[11] J.P. Proot, C. Delerue and G. Allan, Appl. Phys. Lett. 61 (1992) 1948.
[12] B. Delley and E.F. Steigmeier, Phys. Rev. B 47 (1993) 1397.

[13] M. Hirao, T. Uda and Y. Murayama, Mater. Res. Soc. Symp. Proc. 283 (1993) 425; M. Hirao and T. Uda, Surf. Sci. 306 (1994) 87; T. Uda and M. Hirao, J. Phys. Soc. Jpn. 63 B (1994) 97.
[14] B. Delley and E.F. Steigmeier, Appl. Phys. Lett. 67 (1995) 2370.
[15] N.A. Hill and K.B. Whaley, Phys. Rev. Lett. 75 (1995) 1130.
[16] L.W. Wang and A. Zunger, Phys. Rev. Lett. 73 (1994) 1039.
[17] R. Tsu, L. Ioriatti, J.F. Harvey, H. Shen and R.A. Lux, Mater. Res. Soc. Symp. Proc. 283 (1993) 437.
[18] M. Lannoo and G. Allan, Phys. Rev. Lett. 74 (1995) 3415.
[19] L.E. Brus, J. Phys. Chem. 90 (1986) 2555.
[20] D.J. Lockwood, Solid State Commun. 92 (1995) 101; D.J. Lockwood and A.G. Wang, Solid State Commun. 94 (1995) 905; D.J. Lockwood, A. Wang and B. Bryskiewiez, Solid State Commun. 89 (1994) 587.
[21] S. Furukawa and T. Miyasato, Phys. Rev. B 38 (1988) 5726.
[22] W.A. Saunder, H.A. Atwater, K.J. Vahala, R.C. Flagan and P.C. Sercel, Mater. Res. Soc. Symp. Proc. 268 (1993) 118.
[23] H. Takagi, H. Ogawa, Y. Yamazaki, A. Ishizaki and T. Nakagiri, Appl. Phys. Lett. 56 (1990) 2379.
[24] S. Schuppler, S.L. Friedman, M.A. Marcus, D.L. Adler, Y.H. Xie, T.D. Harris, W.L. Brown, Y.J. Chebal, L.E. Brus and P.H. Citrin, Phys. Rev. Lett. 72 (1994) 2648.
[25] L.W. Wang and A. Zunger, Phys. Rev. B, in press.
[26] C.B. Murray, D.J. Norris and M.G. Bawendi, J. Am. Chem. Soc. 115 (1993) 8706.
[27] T. van Buuren, T. Tiedje, J.R. Dahn and B.M. Way, Appl. Phys. Lett. 63 (1993) 2911.
[28] K.A. Mader, L.W. Wang and A. Zunger, Phys. Rev. Lett. 74 (1995) 2555.